Environmental Science and Pollution Research (2021) 28:37520–37533
https://doi.org/10.1007/s11356-021-13202-3

RESEARCH ARTICLE

Electrospun nanofibers of polyvinylidene fluoride incorporated with titanium nanotubes for purifying air with bacterial contamination

Felix Swamidoss Victor[1] · Vaidhegi Kugarajah[1] · Mohan Bangaru[1] · Shivendu Ranjan[2] · Sangeetha Dharmalingam[1]

Received: 15 December 2020 / Accepted: 24 February 2021 / Published online: 13 March 2021

Abstract

Polyvinylidene fluoride (PVDF) blended with varying concentrations of titanium nanotubes (TNT) was electrospun to result in a nanocomposite filter media. Sandwich structures were obtained by depositing the electrospun fibers between polypropylene (PP) nonwoven sheets. The synthesized tubular TNT was confirmed for its morphology through a transmission electron microscope (TEM). The prepared filter media was analyzed through a scanning electron microscope (SEM), X-ray diffraction (XRD), Fourier infrared spectroscopy (FTIR), and thermogravimetric analysis (TGA). The effectiveness of the filter media was evaluated through the zone of inhibition and antibacterial activity against *E. coli* and *S. aureus.* The Box-Behnken design is experimented with three-level variables, namely areal density of substrate (GSM), electrospinning time (hours), and concentration of TNT (wt%) for investigating the bacterial filtration efficiency through an Andersen sampler. Among other statistical tests (STATs), PVDF + 15 wt% TNT has a bacterial filtration efficiency of 99.88% providing greater potentials upon application for clean air management. It can be noted that the future application of this formulation could be efficient filtration of other microbes and could be used in facemasks to industrial-scale air filters.

Keywords Antibacterial filter · Box-Behnken · Bacterial filtration efficiency · Electrospun nanofiber · PVDF · Titanium nanotube

Introduction

Air, widespread with bioaerosols ranging from airborne viruses, bacteria, fungi, to pollens, ensues in various diseases including allergies when inhaled. Low settling velocity and minute size of the particles are the major reason for these particles to remain in the atmosphere for a longer duration than other aerosols (Bush and Portnoy 2001; Kang et al. 2016; Lee and Liao 2014). Bioaerosols have their major contribution in hospitals, poultry farming, waste recycling units involving composting, biotechnology, tanning, etc. The aerosols formed are in the state of suspension for hours which are then transmitted through heat ventilation and air conditioning (HVAC) systems. In general, aerosols can be transmitted through smoke, volatile and organic particles, pollens, dust, etc. (Dhital and Rupakheti 2019; Felix Swamidoss et al. 2019; Mohraz et al. 2019).

A study in 1983 suggested that nearly 34% of microbes in the suburban area are attracted to living systems (Jones and Cookson 1983). Recent advances in filtration show that the advent of nanotechnology in air filters limits the spread of aerosols in HVAC systems. Filtration systems are being developed among which wet scrubbers, electrostatic precipitation, gravity precipitation, and cyclotrons provide high efficiency towards particles less than 1 μm (Tabe 2014), where these approaches are undertaken to either inactivate or eliminate microbial interaction thereby preventing infections. Some of the common attempts include the usage of an electric precipitator, sterilization through ultraviolet radiation, and antibacterial filters (Kang et al. 2016).

Among these approaches, antibacterial filters have high efficiency in air conditioning, air purifiers, ventilating systems which can be applied in two proposed ways, (i) liquid dip

Responsible editor: Philippe Garrigues

✉ Shivendu Ranjan
shivenduranjan@gmail.com

✉ Sangeetha Dharmalingam
sangeetha@annauniv.edu

[1] Department of Mechanical Engineering, College of Engineering (CEG), Guindy Campus, Anna University, Chennai 600 025, India

[2] Faculty of Engineering and the Built Environment, University of Johannesburg, Johannesburg, South Africa

process or (ii) aerosol-based process (Lin and Li 2002; Mainelis et al. 2002). The liquid dip process involves the submersion of the filter in an antibacterial liquid. However, on application of the liquid dip process on high-efficiency particulate air (HEPA) filters, several challenges are faced as HEPA filters are prone to physical deformation and stress. Further pore blockage through the medium may increase the pressure drop of the prepared filter (Yu et al. 2008). The latter, the aerosol-based process, involves the loading of the antibacterial components in the pristine filter thereby integration into a uniform single filter. The mechanism of working is analogous to the conventional air filters in which airborne particles are collected on the filter medium where the promising criterion in these filters is the solid antimicrobial coatings in pristine air filters (Haase et al. 2017; Kang et al. 2016).

Fibrous aerosol filters have been extensively studied due to their high filtration efficiency, uniformity, high surface area, etc. However, the crisis of high energy consumption is of prime concern as far as fibrous filters are considered, as the major requirement in any air filter includes high filtration efficiency and low-pressure drop (Mohraz et al. 2019; Wang et al. 2012). Filtration efficiency increases as the fiber size decreases with respect to the number of fibers present per unit area. Thus, nanofibers have been proven advantageous owing to their low basic weight, small and uniform pore size, and large surface volume ratio. However, due to the fragile structure of nanofibers, a substrate with suitable mechanical stability is essential. In this regard, the application of nonwoven polypropylene (PP) fabrics with appropriate fiber deposition have been investigated for high filtration efficiency with a low-pressure drop (Felix Swamidoss et al. 2019; Selvam and Nallathambi 2015). Electrospinning is a highly active technique used for the formation of nanofibers. When the polymer solution is filled in syringes and allowed to flow through the needle, nanofibers are produced due to the high voltage applied between the tip of the needle and the ground collector (Mollahosseini et al. 2012; Selvam and Nallathambi 2015). The electrospinning apparatus consists of four main parts; syringe holder, high voltage source, feed motor, and rotating drum collector as seen in Fig. 1.

PVDF is a semi crystalline polymer with unique electroactive properties such as piezo, pyro, ferro, flexibility, stability, lightweight, and superior thermal, biocompatible, mechanical properties (Ahn et al. 2013; González et al. 2016; Kesavan et al. 2017; Metcalf et al. 2018). Further, the antibacterial activity can be induced by the addition of inorganic fillers such as silver, titanium, zinc oxide, etc. (Du et al. 2018; Kugarajah and Dharmalingam 2020; Shah et al. 2019). The diverse potential application of titanium corresponding to its chemical stability, high specific area, catalytic activity, and metal support interactions including its superior performance in both alkali and acidic environments has been a subject of continuous interest (Saleh and Gupta 2012). Titanium nanotubes can be synthesized through various methods such as hydrothermal, anodization, sol-gel, and template-assisted methods predominately using titanium dioxide (TiO_2) (Abdullah and Kamarudin 2017; Chouirfa et al. 2019; El Saeed et al. 2015). The facilitation of each method depends on the specific idealistic requirement. Among the above techniques available, the hydrothermal method has been notable due to its production of nanotubes in shorter diameters and safer environment although utilized in elevated temperatures and pressure (Bavykin et al. 2004; Dong et al. 2010; Kugarajah and Dharmalingam 2020; Seo et al. 2001) where the advantages of choosing the hydrothermal method include its eco-friendly nature, simple and inexpensive fabrication (Arruda et al. 2015).

In a report by Xu et al, titanium nanotubes with a diameter of 8–10 nm were synthesized through a hydrothermal method with an operational temperature of 110 °C for 20 h (Xu et al. 2005). Similarly, another study by Abida et al. suggests uniform TNT with an outer diameter of 6–13 nm and a length of 400 nm was obtained with an operational temperature of 130 °C for 20 h (Abida et al. 2011; Bhullar et al. 2019). In the present study, the hydrothermal method was adopted for the synthesis of TNT to obtain nanotubes of low diameter and due to its antimicrobial activity against a broad range of microorganisms (Bardhan et al. 2019; Bartlet et al. 2018; Bhullar et al. 2019; Gunputh et al. 2020; Molina-Reyes et al. 2020; Su et al. 2018; G. Wang et al. 2018) in addition to its inexpensive nature and large surface area (Moongraksathum et al. 2019; Tiyek et al. 2019).

Response surface methodology (RSM) is a statistical tool ideal for experiment designing, optimization of parameters, and evaluation resulting in simultaneous optimization and variation (Sahu et al. 2018). It is an easy approach compared with conventional methods, as it reduces time and produces optimized outcomes in short specific runs. Box-Behnken is a highly efficient three-level design extensively explored owing to its precised outcomes in the determination of process parameters. Also, this method avoids extreme conditions by neglecting the highest and lowest combination which further eases the experiment maintaining the same statistical precision (Bae and Shoda 2005; Ferreira et al. 2007).

In the present research, PVDF incorporated with TNT at varying weight percentages were electrospun on polypropylene nonwoven sheets for the production of smooth nanofibers. The nanofiber was characterized using sophisticated instrumentation methods such as SEM, TEM, XRD, FTIR, and TGA to evaluate the surface morphology, physical, chemical, and thermal characteristics of the nanocomposites. The prepared antibacterial filter media was investigated for its activity against gram-positive *Bacillus subtilis* and gram-negative *Escherichia coli*. The Box-Behnken experimental design was implemented to optimize the best suitable combination for maximizing the bacterial filtration efficiency. The prepared

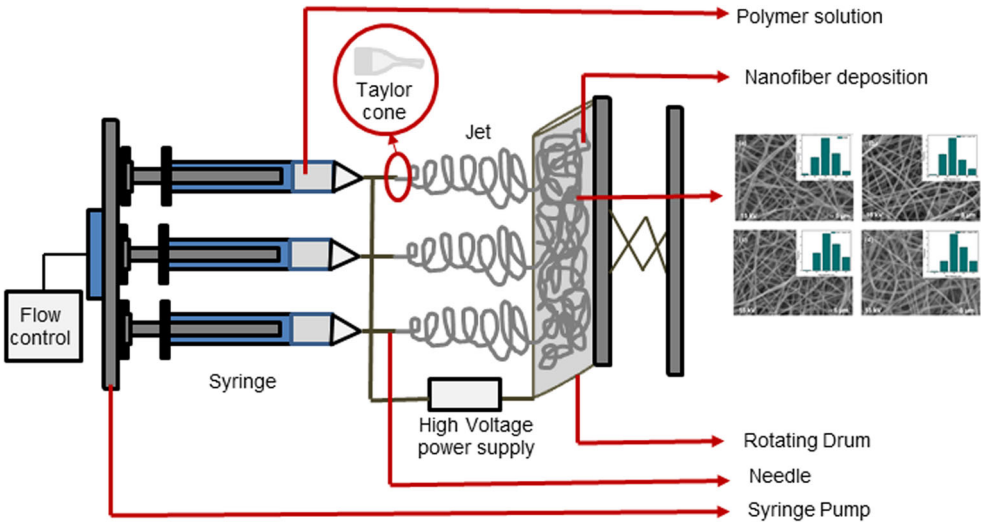

Fig. 1 Schematic representation of electrospinning setup

filter can be applicable in hospitalized environments and as a face mask which is both eco-friendly and cost-effective and could be useful even in this pandemic situation of COVID-19 to filter the virus or trap the breath droplets.

Materials and methods

Materials

Polyvinylidene fluoride (PVDF) (MW = 35000 g/mol) and TiO_2 anatase (25nm) (MW = 79.86 g/mol) was purchased from Sigma Aldrich, Bengaluru, India. Solvents such as Methanol (MW = 32.04 g/mol) and Di Methyl Formamide (DMF) (MW= 73.09 g/mol) and chemicals such as Hydrochloric acid (HCl, 99.5% purity), Sodium Hydroxide pellets (NaOH, 99.5% purity) were procured from SRL Chemical, Chennai, India. Nutrient agar was procured from Sigma Aldrich, Bengaluru, India. *Escherichia coli* (MTCC 443) and *Staphylococcus aureus* (MTCC 3750) were cultured from the pre-culture purchased from Microbial Type Culture Collection (MTCC), Chandigarh, India. All reagents and materials were supplied of analytical grade were used without any further treatments. Double deionized (DI) water (with a measured resistivity of 18.2 MΩ cm^{-1}) was used, throughout the experiments.

Methods

Synthesis of titanium nanotubes

The preparation of titanium nanotubes was conducted as reported earlier (Elumalai et al. 2019; Kugarajah and Dharmalingam 2020). The synthesis was initiated with 4.375 g of titanium dioxide (anatase, 25 nm) dissolved in 10 M NaOH. The solution was subjected to continuous stirring for 30 mins followed by the dispersion of the resultant in an ultrasonicator for the 30 min. The obtained product was then poured into a Teflon lined autoclave and subjected for 24 h at 140 °C. The resultant was neutralized with 1M HCl followed by an aqueous rinse to remove the excess NaOH. Finally, pure TNT was obtained through vacuum filtration.

Preparation of solution for electrospinning

The synthesized TNT at various concentrations (5, 10, 15 wt%) were dispersed in DMF for about 2 h in an ultrasonicator. Initially, a pilot study was performed to determine the concentration of TNT loading. From the results it was observed that increasing the concentration to 20 wt% led to bead formation due to the increase in viscosity of the solution thereby affecting the solution parameter during electrospinning. Hence, the upper limit was set at 15 wt%. To the dispersed solution, 1 g of PVDF was introduced and magnetically stirred continuously for 2 h at 40 °C to avoid any agglomeration resulting in a homogenous solution.

Electrospinning

For the fabrication of the electrospun nanofibers electrospinning machine (PECO, India) was used. The prepared homogenous solution was loaded in three syringes of 2 mL capacity and placed in the aperture of the holder; the tip of the needle is connected to a high voltage power source. The feed motor is connected to a system where the flow rate of the solution through the syringe can be controlled; an aluminum foil is covered over the rotating drum to attract the fibers produced from the tip of the syringe due to high voltage. The drum collector was used to maintain the uniformity of the nanofiber. The operational parameters used in electrospinning are; (i) 10 cm of distance between syringe tip and rotating drum collector; (ii) 0.6 mm inner diameter of

needle; (iii) flow rate 1.5 mL/h; (iv) 25 kV of applied voltage at 25 °C temperature and 45% humidity.

Instrumental characterization

SEM analysis, (JEM-5600 LV, Hitachi Ltd., Tokyo, Japan) of the prepared nanofibers was studied to identify the surface morphology and diameter. The tubular morphology of the synthesized TNT was studied and confirmed through a transmission electron microscope (TEM, TECNAI–T30, Stanford, California, US) with 300 kV and 2 mm resolution. To identify the crystallinity of the prepared nanocomposites, X-ray diffraction (XRD) (Panalytical X'Pert Pro diffractometer, Malvern Panalytical, Malvern, UK) was performed for a scanning rate of 2° per minute at the range between 5 and 70°. FTIR (Alpha Brukar, India) spectroscopy was performed to detect the presence of functional groups in the prepared antibacterial filter media. Pellets of the sample were prepared using KBr and placed on a sample holder for both PVDF and PVDF nanocomposites and scanned for the spectra range between 4000 and 400 cm^{-1}. To determine the thermal stability of the prepared samples TGA (NETZS3 STA 449F3 (TA Instruments, India)) was performed with a scan range of 100 to 600 °C and a heating rate of 20 °C/min. Further, air permeability, pressure drop and pore size of the prepared filter media were studied at SITRA, Coimbatore. A capillary flow porometer CFP-1200A, SITRA and PSGTECHS COE Indutech Laboratory Coimbatore, was used to determine the pore size and distribution in the filter media. Air permeability tester TX3300, SITRA, Coimbatore, was used to measure the flow of air in the prepared filter media, according to ASTM D 737-96 standard with a pressure of 125 Pa (12.7 mm water gauge).

Zone of inhibition

Zone of Inhibition (ZOI) is a vital test to investigate the inhibitory zones produced by prepared filter media against the test bacterium using agar well diffusion method. About 2.8 g of nutrient agar was dissolved in 100 mL of distilled water and autoclaved for 20 min at 121 °C and 15 lbs. The sterilized agar was poured gradually into pre-sterilized petri dishes and was allowed to solidify in a laminar hood. The prepared antibacterial filter media were seeded with a 24-h culture of bacterial strains (*E.coli*-443 and *S.aureus*-3750). Wells were cut and different concentration of PVDF + TNT (5, 10 and 15 wt%) was added. The plates were then incubated at 37 °C for 24 h. The antibacterial activity was assayed by measuring the diameter of the inhibition zone formed around the wells.

Antibacterial activity

The antibacterial test was tested to evaluate the efficiency of the developed filter media in accordance with our earlier report (Felix Swamidoss et al. 2019). The experimental procedure is as follows: About 5 mL of sterilized nutrient broth was prepared by standard protocols. Antibacterial activity was measured for both control and test samples which were introduced in Luria broth (LB) with 1×10^5 colonies forming unit per mL (CFU/mL) which was incubated at 37 °C for colony growth. The number of colonies was calculated for 7 h at regular intervals. Antibacterial activity of the given sample was determined using the following formula:

$$\frac{B-A}{B} \times 100 = R\% \quad (1)$$

where the reaction rate is denoted by R; A represents the CFU/mL of the test sample and B represents the CFU/mL of the control.

Experimental design

The Box-Behnken experimental design was adopted for the present study owing to its advantage in precision from the factor variables that are equidistant from the center points for optimizing the parameters. The preparation of bacterial filter media depends on the substrate utilized, the polymer blend solution, and the electrospinning time. Thus, the Box-Behnken design was set with three variables including areal density, electrospinning time, and concentration of TNT as seen in Table 1, which resulted in 15 statistical runs (STATs)

Bacterial filtration efficiency

To calculate the bacterial filtration efficiency, the prepared filter medium was tested according to ASTM F 2101 using *S. aureus* as test aerosol. Aerosols of particle size in the range 0.1–10 μm with a constant flow rate of 27.3 L/min were pumped and loaded in a nebulizer under a face velocity of 20 cm/s. Before the test, the samples of *S. aureus* were kept for about 4 h at 21 °C and 85% humidity by dissolving in 1.5% peptone water with a yield level of 2200 ± 500 CFU/mL. To determine the filtration efficiency, Andersen sampler was utilized as represented in Fig. 2 (Felix Swamidoss et al. 2019; King and McFarland 2012). Andersen Sampler works under the principle of inertial impaction incorporated with six

Table 1 Process parameters obtained through the Box-Behnken design

Variables	Process parameters	Levels		
		− 1	0	+ 1
X_1	Areal density (grams per sq. meter (GSM))	40	60	80
X_2	Electrospinning time (hrs)	1	2	3
X_3	TNT (wt%)	5	10	15

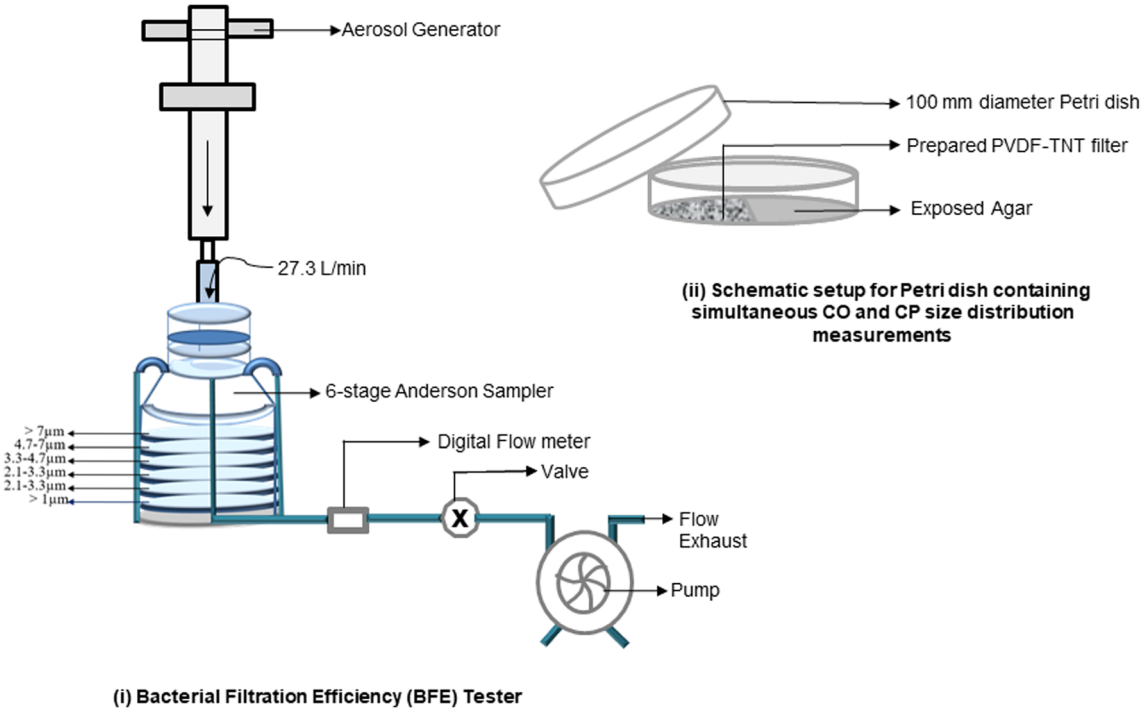

Fig. 2 Schematic representation of (i) setup for bacterial filtration efficiency tester and (ii) Petri dish displaying both CP and CO size distribution measurements

staged perforated plate aerosol fractions with a range from 7 to < 1 μm. The effect of bacteria transitory through the prepared sampler was studied with the aid of pre-sterilized nutrient agar plates upon which prepared filter was introduced on one half under each perforated plate. As the bacterial aerosol passes through the sampler, bacteria are imposed on the six stages of agar plates for 48 h at 37 °C, which are further incubated. Thus, by standard microbiological techniques for counting the culturable organisms (CO) obtained in the agar plate or the culturable particulates (CP) obtained in the perforated plate where the prepared filter is placed, the colony-forming units (CFU) of the test and control sample was determined according to Eq. (2) wherein the determination of the aerosol size distribution in terms of CO or CP was performed:

$$\frac{N_i}{N} = n_i \tag{2}$$

where N_i is the number of CP present in the first stage; N is the number of CP present in all stages.

Further, the bacterial filtration efficiency (BFE) tests in addition to the STATs were performed for both controls (Polypropylene nonwoven sheet without PVDF) and with sample (Polypropylene nonwoven with PVDF) was performed. All experiments were performed in triplicate to analyze the efficiency of the obtained results. The bacterial filtration efficiency can be calculated by finding the difference in the control sample (PP + PVDF) and the test sample (PVDF = various wt% TNT).

$$\left(\frac{C-T}{C}\right)*100 = BFE\% \tag{3}$$

where

C is the CFU/mL of the control
T is the CFU/mL of the test sample

Results and discussion

Morphological studies

Scanning electron microscopy (SEM) was studied to determine the morphology of the synthesized TNT. Figure 3a represents the successful conversion of TiO_2 to TNT through hydrothermal treatment. Further TNT established bundled arrangement with tubular morphology similar to other reports (Bavykin et al. 2004; Manfroi et al. 2014; Van Viet and Thi 2016), with an average diameter of 38–58 nm analyzed using the ImageJ software (Kugarajah and Dharmalingam 2020; Seo et al. 2001). Figure 3b and c represent the TEM images confirming the tubular arrangement of the synthesized TNT at different magnifications. From the images, the intact and hollow nature of the synthesized TNT was confirmed (Khaled

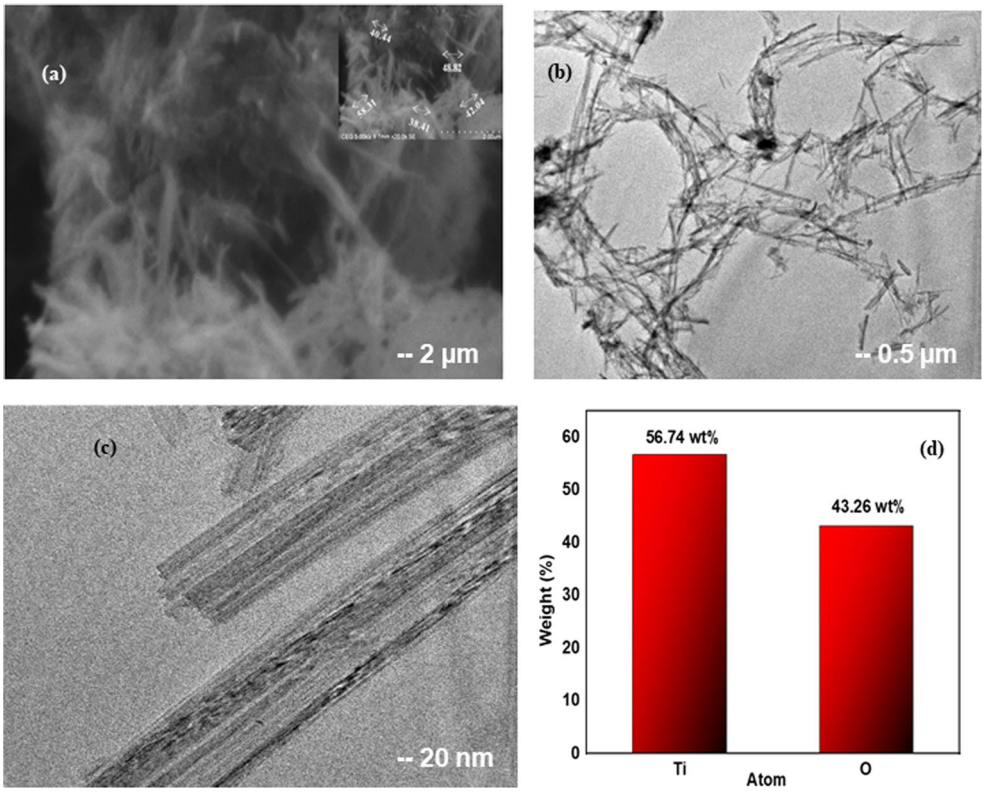

Fig. 3 **a** SEM image of TNT. TEM image of TNT at **b** 0.5 µm and **c** 20 nm. **d** EDAX of TNT

et al. 2007; Plodinec et al. 2014; Yuan and Su 2004). Figure 3d represents the elemental composition of TNT through EDAX analysis confirming the absence of other impurities.

SEM morphologies with varying concentrations (5, 10, and 15 wt%) of TNT are represented in Fig. 4. The average fiber diameter of PVDF (Fig. 4a) was found to be 286 nm in agreement with our earlier report (Felix Swamidoss et al. 2019). With the incorporation of TNT in the base solution, the fiber diameter was found to decrease with the increase in the concentration of TNT to 265, 234, and 193 nm as seen in Fig. 4b–d thereby increasing the surface area. The decrease in fiber diameter can be inferred to the increase in charge density of the naïve polymer. The reduction in fiber diameter reducing the pore size can also be attributed to the transportation of fiber under the electric field which had a large impact on elongation and stretching. The decreased pore size increases the proportion of particle capture (Santos and Bedrikovetsky 2004; Selvam and Nallathambi 2015).

X-ray diffraction

The XRD diffractograms of the PVDF and PVDF + various wt% of TNT nanofibers are depicted in Fig. 5(a–d). A characteristic broad peak at the range between 2θ = 20–25° was observed in all prepared filter media. The intensity of the broad peak was found to decrease with the increase in TNT concentration similar to a report by Shah et al. The reduction in the peak intensity can be associated with the physical forces between the polymer and filler thereby reducing the interactions in between (Shah et al. 2019). The addition of TNT in the polymer backbone with uniform dispersion led to the variation in the XRD profile. The hydrothermal treatment led to the conversion of the crystalline phase of TNT into a monoclinic phase which was further modified when incorporated in PVDF which led to the decrease in crystallinity (Ingale et al. 2016; Nada et al. 2014; Padiyan and Raja 2012).

Fourier transform infrared spectroscopy

PVDF and PVDF+TNT (various wt%) nanofibers were analyzed to investigate the presence of functional groups through FTIR analysis as seen in Fig. 6(a–d). Ideally, PVDF may exist in the semi-crystalline phase. In the spectrum of plain PVDF, β phase peaks were observed in 563 and 840 cm^{-1}which are attributed to the C-F stretching vibrations. Other characteristic absorption bands at 3019 and 1496 cm^{-1} corresponded to the CH_2 symmetric and asymmetric vibrations. A wagging vibration was also observed at 1383 cm^{-1}. In addition to the above, peaks at 880 and 841 cm^{-1} corresponded to C-F and C-C stretching vibration of PVDF. The obtained results were in accordance with earlier reports (Felix Swamidoss et al. 2019; Issa et al. 2017).

The chemical structure of the prepared blend exhibited the characteristic peaks of PVDF. For example, peaks such as 880 and 841 cm^{-2} were retained. A broad range

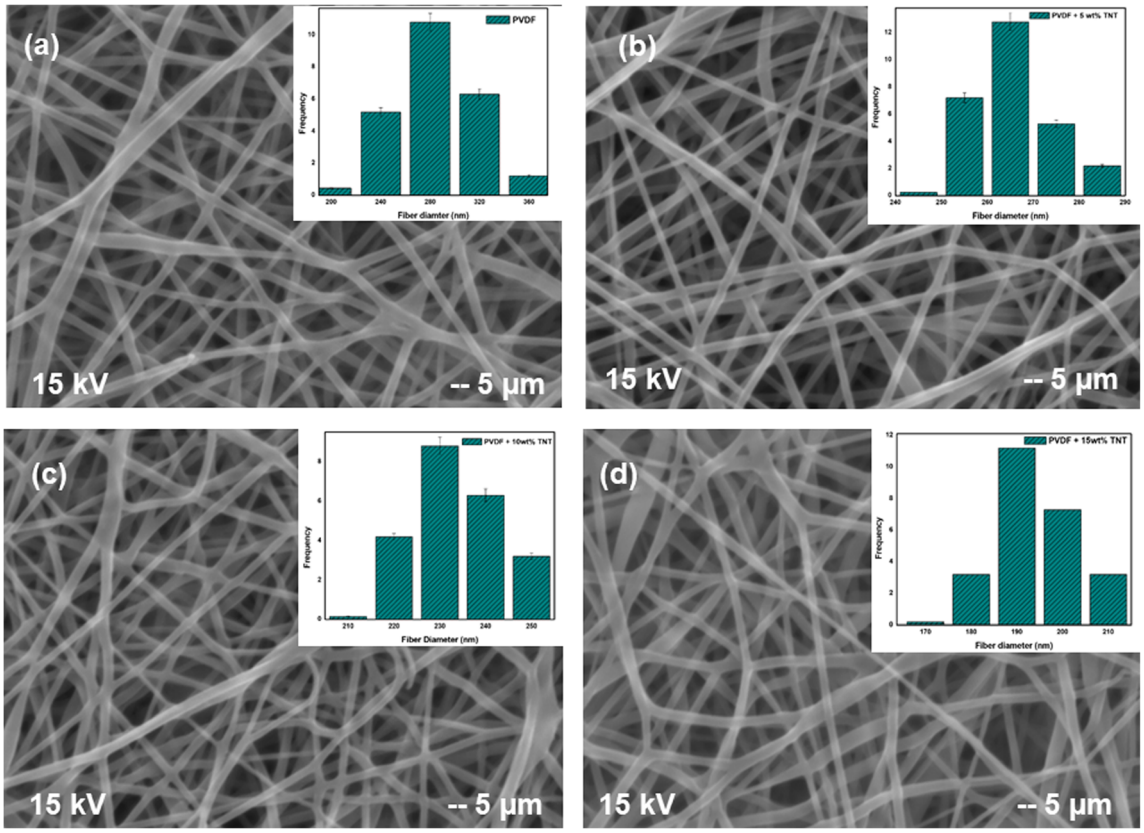

Fig. 4 SEM images of **a** PVDF, **b** PVDF + 5 wt% TNT, **c** PVDF + 10 wt% TNT, and **d** PVDF + 15 wt% TNT

of peaks around 500 to 900 cm^{-1} contributed to the Ti-O stretching of the TNT skeleton. The peak around 2800–3100 cm^{-1} may be attributed to stretching and bending vibrations of the O-H present on the tubular structured TNT. A band stretch around 1400–1500 cm^{-1} contributed to the vibrations of hydroxyl and absorbed water molecules. The obtained results were in accordance with earlier reports (Elumalai et al. 2019; Kugarajah and Dharmalingam 2020; Shah et al. 2019).

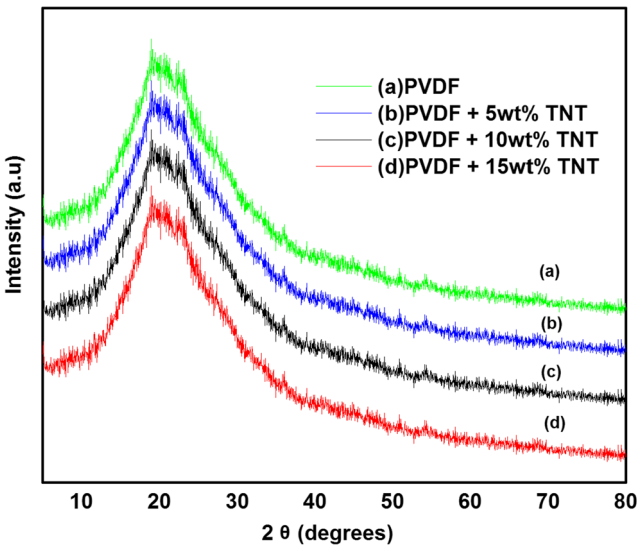

Fig. 5 XRD patterns of (a) PVDF, (b) PVDF + 5 wt% TNT, (c) PVDF + 10 wt% TNT, and (d) PVDF + 15 wt% TNT

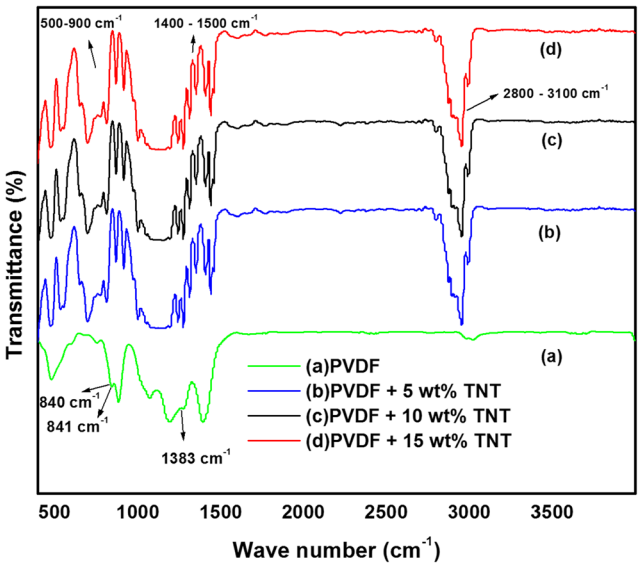

Fig. 6 FTIR spectra of (a) PVDF, (b) PVDF + 5 wt% TNT, (c) PVDF + 10 wt% TNT, and (d) PVDF + 15 wt% TNT

Thermal gravimetric analysis

The thermal stability of nanofibers was tested to ensure its stability during utilization at various applications and for further reuse (Bai et al. 2012; Felix Swamidoss et al. 2019). TGA thermograms of electrospun PVDF and PVDF with varying TNT wt% are depicted in Fig. 7(a–d). From the figure, it was inferred that the thermogram of PVDF (Fig. 7(a)) was stable up to 350 °C whereas upon addition of various concentrations of TNT (wt%) the prepared filter media were susceptible to changes as seen in Fig. 7. Figure 7(a) shows that pristine electrospun PVDF exhibited a single step degradation, where HF present in the polymer backbone evaporated resulting in CH=CF-CH=CF conjugations (Zucolotto et al. 2004).

From Fig. 7(b–d), it was observed that electrospun nanocomposite fibers exhibited a similar trend as pristine polymers. However, the stability of the filter media was found to increase. The shift can be elaborated due to the enhanced interactions between PVDF and TNT as reported earlier (Shah et al. 2019). It was observed that the degradation temperature (T_d) shifted from 350 °C (plain PVDF) to 410 °C (PVDF + 5 wt% TNT). Minimal mass losses at the initial stages were also inferred indicating the cleavage of the hydroxyl bonds in TNT. The weight loss was observed to be shifted to 465.8 °C for PVDF + 10 wt% TNT and 465 °C for PVDF + 15 wt% TNT corresponding to the addition of TNT wt% in electrospun PVDF. The enhanced thermal properties of TNT led to the delay of PVDF main chain decomposition thereby improving the thermal stability of the prepared filter media (Hanaor and Sorrell 2011).

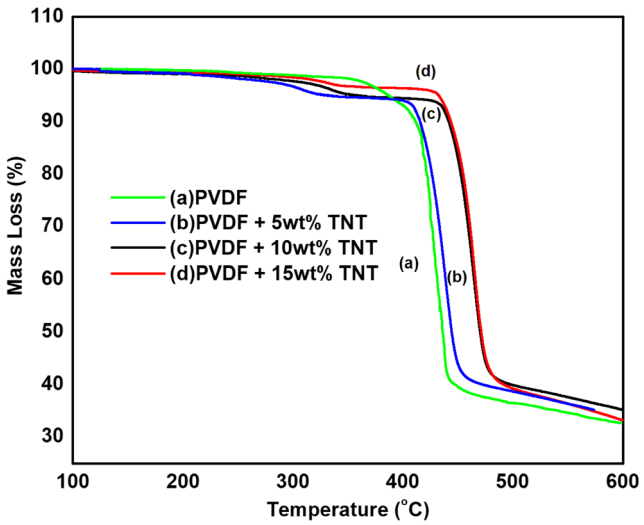

Fig. 7 TGA curve of (a) PVDF, (b) PVDF + 5 wt% TNT, (c) PVDF + 10 wt% TNT, and (d) PVDF + 15 wt% TNT

Zone of inhibition

Zone of inhibition for the prepared filter was tested against *E. coli* and *S. aureus* for PVDF+TNT (various wt%) where pristine PVDF was applied as the control. The experiment was run in triplicate and the average results produced by the zone of inhibition were accorded in Fig. 8a, b. It was observed that a minimal zone was obtained for pure PVDF owing to its inbuilt electrostatic property on both gram-positive and negative species. Upon TNT addition, the clear zones of inhibition were obtained in accordance with earlier reports (Bartlet et al. 2018; Chouirfa et al. 2019; Li et al. 2013; G. Wang et al. 2018; Zhao et al. 2013). The bactericidal activity increased with increasing concentration of TNT which was due to the characteristic antibacterial property of TNT (Fig. 8c). The antimicrobial components present in the TNT diffuse out into the medium and interacts with the test organisms. The mechanism of antibacterial activity can be justified as follows: TNT binds with the negatively charged bacterial cell wall, which leads to a structural modification resulting in bacterial cell wall degradation, thereby inhibiting bacterial growth (Li et al. 2013). The resulting zones of inhibition formed were random as there was a confluent lawn of growth. The diameter of zone of inhibition was measured in millimeters which showed that the increasing TNT concentration increased the antibacterial activity.

The antibacterial activity of pure PVDF and PVDF-TNT with respect to colonies forming unit at regular intervals were investigated within 7 h which are represented in Fig. 9 (i) and (ii). In accordance with the zone of inhibition, PVDF produced minimal antibacterial activity. With an increase in TNT concentration, the antibacterial activity increased as shown in Fig. 9 (i, ii). From the graph, it was evident that 15 wt% of the TNT blend showed maximum antibacterial activity due to higher TNT loading within the respective period.

Bacterial filtration efficiency

The prepared filter media was tested for its bacterial filtration efficiency with *S. aureus* as the test aerosol under ASTM F 2101 standard protocol using an Anderson sampler and the results of BFE are tabulated through Box-Behnken experimental design is represented in Table 2. When air containing bacteria passes through the six staged sampler, bacteria either retain/penetrate through the medium with respect to the sieve size in each stage of the sampler; thus, the CO or CP was calculated through Eq. (2). The bacterial filtration efficiency was calculated by substituting the results of Eq. (2) on Eq. (3). The maximum BFE of 99.88 % was obtained for PVDF + 15 wt% TNT. The obtained efficiency can be inferred to the high concentration of TNT, reduced fiber diameter enabling better particle capture. The contribution of each parameter

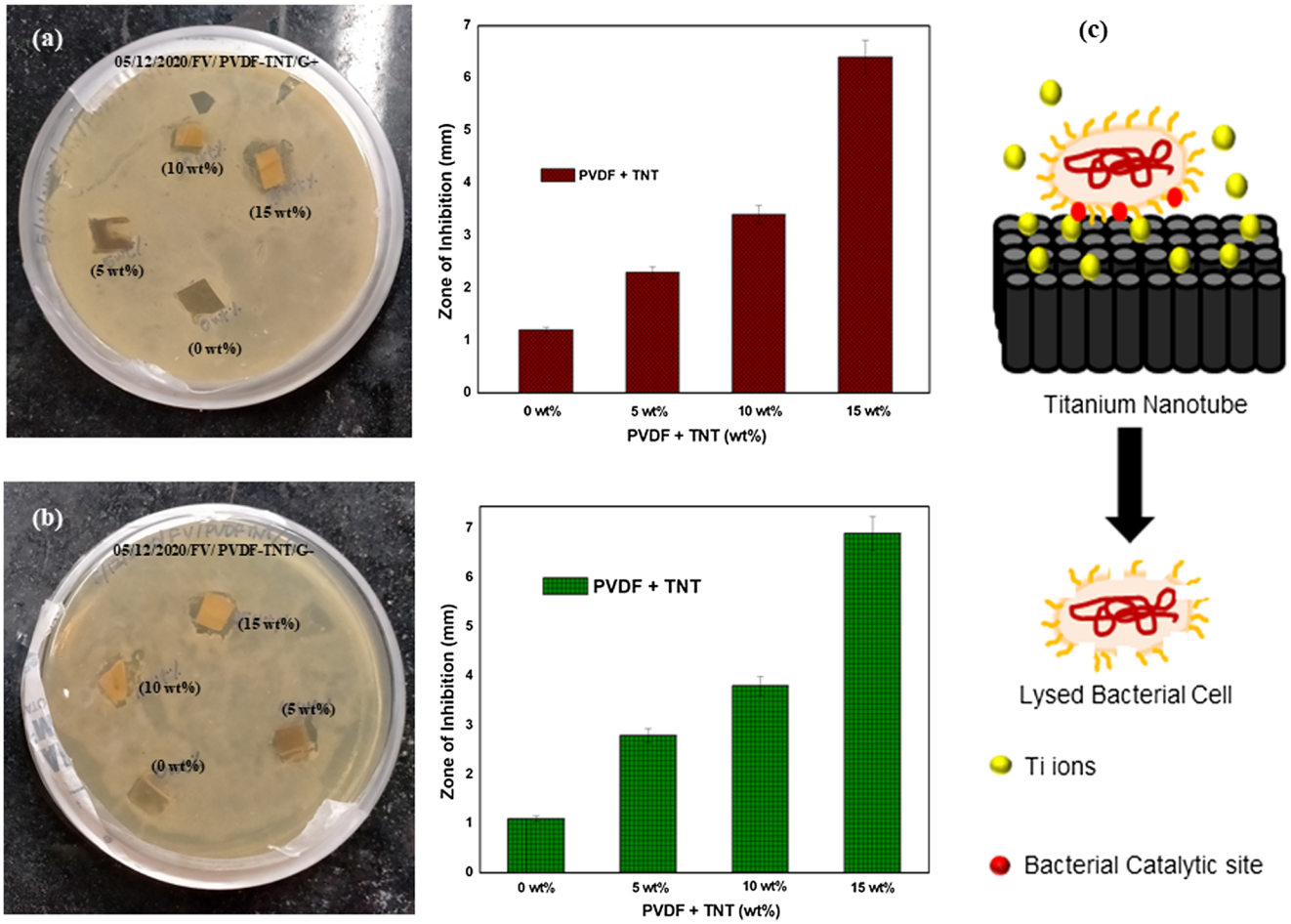

Fig. 8 Zone of inhibition (ZOI) of prepared nanocomposites against **a** *E. coli* and **b** *S. aureus*. **c** Mechanism of TNT against bacteria

selected in the study was explored by investigating the influence of the areal density of the substrate, electrospinning time, and the concentration of TNT on bacterial filtration efficiency through contour plots and surface plots as shown in Fig. 10. Further, the ANOVA table as seen in Table S1 suggests the interaction between the selected parameters through which an empirical equation as seen in Table 2 was obtained. In addition, Table 2 also shows the BFE of the areal density without the addition of the prepared filter media to elaborate on the enhanced antibacterial effect. Further, major characteristics such as pore size, air permeability, and the pressure drop obtained for various combinations were tabulated. It was

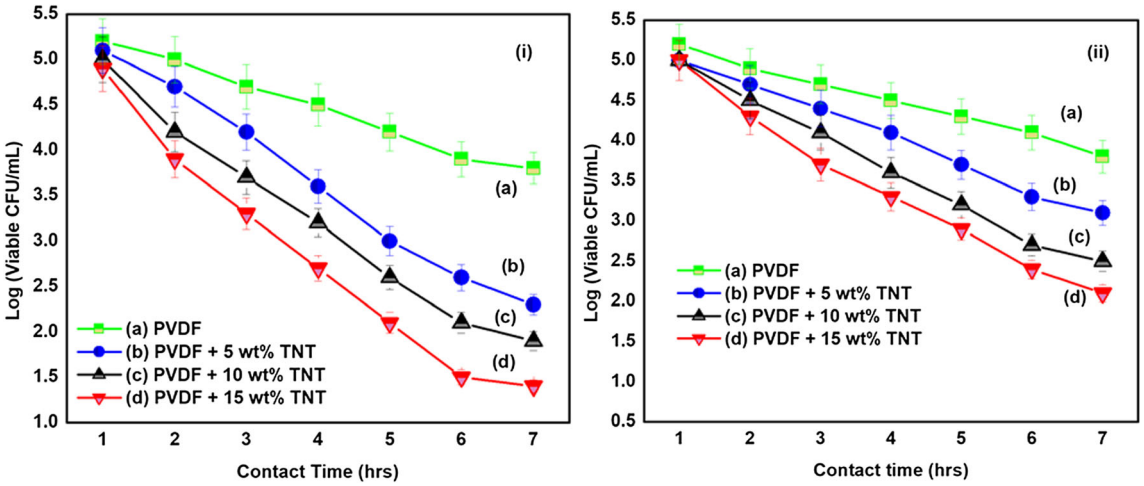

Fig. 9 (i) Antibacterial activities against *E. coli* and (ii) Antibacterial activities against *B. subtilis*

Table 2 Bacterial filtration efficiency produced through the experimental runs

S. no.	Sample ID	Areal density (GSM)	Electrospinning time (hrs)	TNT (wt%)	Filtration efficiency (%)	Air permeability ($cm^3/cm^2/s$)	Pore size (μm)	Porosity (%)	Pressure drop (mm of H_2O)	Rank
1	STATT14	60	2	10	92.98	122.75	5.53	73.2	5.72	5
2	STAT15	60	2	10	92.94	118.96	5.11	73.3	4.61	7
3	STAT8	80	2	15	98.70	98.25	2.51	72.3	6.52	2
4	STAT10	60	3	5	88.74	103.63	4.29	64.7	5.87	10
5	STAT1	40	1	10	82.21	136.11	7.03	87.9	2.73	14
6	STAT7	40	2	15	93.99	126.13	5.34	75.1	4.12	4
7	STAT3	40	3	10	91.40	105.71	4.11	69.8	5.73	8
8	STAT4	80	3	10	96.85	93.05	2.71	65.9	6.72	3
9	STAT9	60	1	5	79.35	137.08	6.73	79.8	3.12	15
10	STAT5	40	2	5	83.14	127.62	6.15	77.5	2.94	13
11	STAT13	60	2	10	92.96	119.01	5.15	73.2	4.32	6
12	STAT11	60	1	15	90.75	133.58	6.91	81.1	2.87	9
13	STAT6	80	2	5	87.05	109.62	3.49	76.3	3.62	11
14	STAT2	80	1	10	86.43	134.53	6.53	81.5	3.35	12
15	STAT12	60	3	15	99.88	91.35	1.91	63.5	6.94	1
16	STAT 16	40 GSM PP nonwoven sheet			42.10	109.71	11.56	95.7	5.12	18
17	STAT 17	60 GSM PP nonwoven sheet			44.78	105.63	11.01	93.1	6.12	17
18	STAT 18	80 GSM PP nonwoven sheet			46.31	105.05	9.15	91.4	6.31	16
	Std. dev.	0.413	**R^2**		99.83					
	Mean	90.44	**Adjusted R^2**		99.53					
			Predicted R^2		97.36					
Bacterial filtration efficiency (BFE)		= 42.67 + 0.4710 areal density (GSM) + 13.584 electrospinning time (hrs) + 1.754 TNT (wt%) − 0.003388 areal density (GSM)*areal density (GSM) − 2.403 electrospinning time (hrs)*electrospinning time (hrs) − 0.03590 TNT (wt%) * TNT (wt%) + 0.01537 areal density (GSM)*electrospinning time (hrs) + 0.00193 areal density (GSM)* TNT (wt%) − 0.0130 electrospinning time (hrs) * TNT (wt%)								

observed that the pore size and air permeability reduced with the increase in TNT wt% and electrospinning time which attributed to the increase in packing density of the fibers. From Table 2, it was observed that STAT 12 possessed the minimum pore size of 1.91 μm with reduced air permeability of 91.35 $cm^3/cm^2/s$ with an increased pressure drop (6.94 mm of H_2O) compared with STAT 1 which had a pore size of 7.03 μm, air permeability of 136.11 $cm^3/cm^2/s$, and decreased pressure drop of 2.73 mm of H_2O. From the obtained results, it was observed that the air permeability was directly proportional to pore size, whereas the pressure drop was inversely proportional to the pore size. From Table 2, it was inferred that the BFE was found to increase with an increase in the concentration of TNT (wt%) suggesting that even a minimal dosage of TNT had a major impact on filtration efficiency. The obtained result was in correlation to other reports with silver as an antibacterial agent (Felix Swamidoss et al. 2019; Selvam and Nallathambi 2015).

Increasing individual factors increase the BFE; however, the order of increase was found to vary depending on discrete variables in the order of concentration of TNT, electrospinning time, and areal density of the substrate. From Table 2, it was observed that STAT 12 produced the maximum filtration efficiency of 99.88% with 60 GSM, 3 h of electrospinning, and 15 wt% of TNT whereas STAT 10 showed 88.74% with 60 GSM, 3 h of electrospinning, and 5 wt% TNT. It was observed that a filtration efficiency of about +20 % was observed when the TNT concentration was 15 wt% as shown in Fig. 10 (i–vi). However, it was also observed that the areal density did not have a comparatively major impact on efficiency. The impact of TNT concentration can be further justified through the plots (Fig. 10 (ii, iii)).

The effect of electrospinning time on BFE can be elaborated through the obtained contour plot and surface plots as shown in Fig. 10. From Table 2, it was observed that a maximum BFE of 79.35% (STAT 9) was obtained with 1 hr of electrospinning time and 5 wt% TNT whereas a BFE of 90.75% (STAT 11) was obtained with 1 hr electrospinning time and 15 wt% TNT. When the electrospinning time was further increased to 3 h a maximum BFE of 99.88% was obtained as shown in the surface plots.

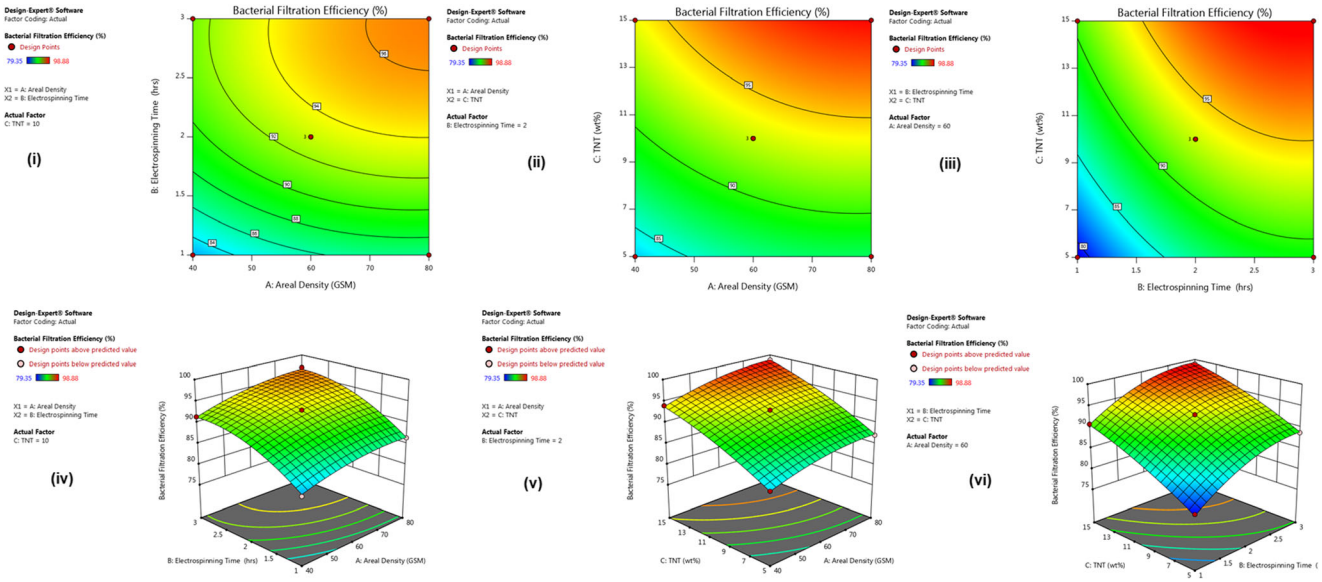

Fig. 10 Contour and Surface plots obtained for the input parameters against BFE

The overall responses obtained through the experimented design are tabulated below in the ANOVA Table S1. The model *F*-value of 1005 implies the model was significant confirming the suitability of the obtained equation. It is also observed that the p values are less than 0.001, indicating that the parameters were significant. Figure S1 represented the graphical representation of actual versus predicted values. Nonlinear relationships between parameters are essential to evaluate the predominance of individual factors.

In summary, it was observed that the efficiency of the antibacterial filter mainly depends on the TNT wt% and electrospinning time. Based on the filtration efficiency the experimental levels were ranked and shown in Table 2 and STAT 12 shows the highest efficiency of 99.88%, which was higher compared with certain earlier reported research as seen in Table 3. The parameters of STAT 12 were used to obtain the correlation factor R^2 as 99.83. Overall, it was seen that PVDF + 15 wt% TNT with 3 h of electrospinning time and 60 GSM of substrate possessed a bacterial filtration efficiency of 99.88% with good antibacterial property against both gram-positive and negative organisms.

Conclusion

A novel antibacterial filter comprising electrospun PVDF and TNT was explored for antibacterial filtration. The successful conversion of TiO_2 into TNT was confirmed through TEM for its tubular morphology. The prepared nanofibers were characterized by SEM, FTIR, XRD, and TGA analysis. The Box-Behnken experimental design was adopted to optimize the best possible result and the outcome was investigated through

Table 3 Certain earlier reported electrospun filter media for bacterial filtration

S. no.	Electrospun filter media	BFE (%)	Reference
1	Poly acrylonitrile/Ag	99	(Karthick and Gobi 2017)
2	Poly vinyl alcohol (PVA)/poly (acrylic acid) PAA	98	(Zhu et al. 2018)
3	Multifunctional TiO_2/poly acrylonitrile	96.75	(Chen et al. 2019)
4	Poly(vinyl alcohol-*co*-ethylene) (EVOH)/dimethylol-5,5-dimethylhydantoin (DMDMH)	99.5	(Liang et al. 2019)
5	PVA/chitosan/3-allyl-5,5-dimethylhydantoin (ADMH)	99.3	(Zhang et al. 2020)
6	PAN/ Ag	99	(Selvam and Nallathambi 2015)
7	PVDF + 15 wt% Ag	99.86	(Felix Swamidoss et al. 2019)
8	PVDF + 15 wt% TNT	99.88	In this study

15 experimental runs. Antibacterial and zone of inhibition studies revealed that the prepared filter media was highly efficient against both gram-positive and gram-negative strains. From the surface and contour plots it was observed that even when minimal TNT concentration and electrospinning time was provided, a major impact on the bacterial filtration efficiency was observed compared with the areal density. In this study, it was found that 15 wt% of the filler proved for the highest bacterial filter efficiency of 99.88% with 3 h of electrospinning time and 60 GSM of the nonwoven sheet. The present study opens a pathway for a novel combination of highly effective filter media which can be applied in the production of facemasks.

Supplementary Information The online version contains supplementary material available at https://doi.org/10.1007/s11356-021-13202-3.

Author contribution Felix Swamidoss and Vaidhegi Kugarajah: conceptualization, methodology, software. Felix Swamidoss and Vaidhegi Kugarajah: data curation, writing—original draft preparation. Mohan Bangaru, Shivendu Rajan, and Sangeetha Dharmalingam: visualization, investigation. Mohan Bangaru, Shivendu Rajan, and Sangeetha Dharmalingam: supervision. Felix Swamidoss and Vaidhegi Kugarajah: software, validation. Mohan Bangaru, Shivendu Rajan, and Sangeetha Dharmalingam: writing—reviewing and editing.

Funding This study was financially supported by the Indian Council of Medical Research (ICMR) (Letter No. 5/20/16/Bio/2013-NCD-1, dated 27.03.2015) and the Department of Biotechnology (DBT) (Letter No. BT/PR12574/PBD/26/437/2014, dated 21.06.2016), New Delhi, India.

Data availability The raw/processed data required to reproduce these findings cannot be shared at this time as the data also forms part of an ongoing study.

Declarations

Ethics approval and consent to participate Not applicable

Consent for publication Not applicable

Competing interests The authors declare no competing interests.

References

Abdullah M, Kamarudin SK (2017) Titanium dioxide nanotubes (TNT) in energy and environmental applications: an overview. Renew Sust Energ Rev 76:212–225. https://doi.org/10.1016/j.rser.2017.01.057

Abida B, Chirchi L, Baranton S, Napporn TW, Kochkar H, Léger J-M, Ghorbel A (2011) Preparation and characterization of Pt/TiO2 nanotubes catalyst for methanol electro-oxidation. Appl Catal B Environ 106(3–4):609–615

Ahn Y, Lim JY, Hong SM, Lee J, Ha J, Choi HJ, Seo Y (2013) Enhanced piezoelectric properties of electrospun poly (vinylidene fluoride)/multiwalled carbon nanotube composites due to high β-phase formation in poly (vinylidene fluoride). J Phys Chem C 117(22): 11791–11799

Arruda LB, Santos CM, Orlandi MO, Schreiner WH, Lisboa-Filho PN (2015) Formation and evolution of TiO2 nanotubes in alkaline synthesis. Ceram Int 41(2):2884–2891

Bae S, Shoda M (2005) Statistical optimization of culture conditions for bacterial cellulose production using Box-Behnken design. Biotechnol Bioeng 90(1):20–28

Bai H, Wang X, Zhou Y, Zhang L (2012) Preparation and characterization of poly(vinylidene fluoride) composite membranes blended with nano-crystalline cellulose. Prog Nat Sci Mater Int 22(3):250–257. https://doi.org/10.1016/j.pnsc.2012.04.011

Bardhan S, Pal K, Roy S, Das S, Chakraborty A, Karmakar P, Basu R, Das S (2019) Nanoparticle size-dependent antibacterial activities in natural minerals. J Nanosci Nanotechnol 19(11):7112–7122

Bartlet K, Movafaghi S, Dasi LP, Kota AK, Popat KC (2018) Antibacterial activity on superhydrophobic titania nanotube arrays. Colloids Surf B: Biointerfaces 166:179–186

Bavykin DV, Parmon VN, Lapkin AA, Walsh FC (2004) The effect of hydrothermal conditions on the mesoporous structure of TiO 2 nanotubes. J Mater Chem 14(22):3370–3377

Bhullar SK, Ruzgar DG, Fortunato G, Aneja GK, Orhan M, Saber-Samandari S, Sadighi M, Ahadian S, Ramalingam M (2019) A facile method for controlled fabrication of hybrid silver nanoparticle-poly (-caprolactone) fibrous constructs with antimicrobial properties. J Nanosci Nanotechnol 19(11):6949–6955

Bush RK, Portnoy JM (2001) The role and abatement of fungal allergens in allergic diseases. J Allergy Clin Immunol 107(3 Suppl):S430–S440. https://doi.org/10.1067/mai.2001.113669

Chen K-N, Sari FNI, Ting J-M (2019) Multifunctional TiO2/polyacrylonitrile nanofibers for high efficiency PM2. 5 capture, UV filter, and anti-bacteria activity. Appl Surf Sci 493:157–164

Chouirfa H, Bouloussa H, Migonney V, Falentin-Daudré C (2019) Review of titanium surface modification techniques and coatings for antibacterial applications. Acta Biomater 83:37–54

Dhital S, Rupakheti D (2019) Correction to: Bibliometric analysis of global research on air pollution and human health: 1998–2017. Environ Sci Pollut Res 26(24):25386. https://doi.org/10.1007/s11356-019-05792-w

Dong B, He B, Chai Y, Liu C (2010) Novel Pt nanoclusters/titanium dioxide nanotubes composites for hydrazine oxidation. Mater Chem Phys 120(2–3):404–408

Du Q, Wei D, Liu S, Cheng S, Hu N, Wang Y, Li B, Jia D, Zhou Y (2018) The hydrothermal treated Zn-incorporated titania based microarc oxidation coating: Surface characteristics, apatite-inducing ability and antibacterial ability. Surf Coat Technol 352:489–500

El Saeed AM, Abd El-Fattah M, Dardir MM (2015) Synthesis and characterization of titanium oxide nanotubes and its performance in epoxy nanocomposite coating. Prog Org Coat 78:83–89

Elumalai V, Deenadhayalan T, Asitha AK, Kirubhakaran DJ, Sangeetha D (2019) Preparation of tungstic acid functionalized titanium oxide nanotubes and its effect on proton exchange membrane fuel cell. SN Appl Sci 1(4):348

Felix Swamidoss V, Bangaru M, Nalathambi G, Sangeetha D, Selvam AK (2019) Silver-incorporated poly vinylidene fluoride nanofibers for bacterial filtration. Aerosol Sci Technol 53(2):196–206

Ferreira SL, Bruns RE, Ferreira HS, Matos GD, David JM, Brandao GC, da Silva EG, Portugal LA, dos Reis PS, Souza AS, dos Santos WN (2007) Box-Behnken design: an alternative for the optimization of analytical methods. Anal Chim Acta 597(2):179–186. https://doi.org/10.1016/j.aca.2007.07.011

González LF, Joubert A, Andrès Y, Liard M, Renner C, Le Coq L (2016) Filtration performances of HVAC filters for PM10 and microbial aerosols— Influence of management in a lab-scale air handling unit. Aerosol Sci Technol 50(6):555–567. https://doi.org/10.1080/02786826.2016.1167833

Gunputh UF, Le H, Lawton K, Besinis A, Tredwin C, Handy RD (2020) Antibacterial properties of silver nanoparticles grown in situ and

anchored to titanium dioxide nanotubes on titanium implant against Staphylococcus aureus. Nanotoxicology 14(1):97–110
Haase H, Jordan L, Keitel L, Keil C, Mahltig B (2017) Comparison of methods for determining the effectiveness of antibacterial functionalized textiles. PLoS One 12(11):e0188304
Hanaor DAH, Sorrell CC (2011) Review of the anatase to rutile phase transformation. J Mater Sci 46(4):855–874
Ingale SV, Wagh PB, Sastry PU, Basak CB, Bandyopadhyay D, Phapale SB, Gupta SC (2016) Studies on impact sensitivity of nanosized trinitrotoluene (TNT) confined in silica processed by sol-gel method. Defence Technol 12(1):46–51
Issa AA, Al-Maadeed MA, Luyt AS, Ponnamma D, Hassan MK (2017) Physico-mechanical, dielectric, and piezoelectric properties of PVDF electrospun mats containing silver nanoparticles. C—Journal Carbon Res 3(4):30
Jones BL, Cookson JT (1983) Natural atmospheric microbial conditions in a typical suburban area. Appl Environ Microbiol 45(3):919–934. https://doi.org/10.1128/AEM.45.3.919-934.1983
Kang JS, Kim H, Choi J, Yi H, Seo SC, Bae G-N, Jung JH (2016) Antimicrobial air filter fabrication using a continuous high-throughput aerosol-based process. Aerosol Air Qual Res 16(8):2059–2066. https://doi.org/10.4209/aaqr.2015.10.0598
Karthick SA, Gobi N (2017) Nano silver incorporated electrospun polyacrylonitrile nanofibers and spun bonded polypropylene composite for aerosol filtration. J Ind Text 46(6):1342–1361
Kesavan JS, Humphreys PD, Bottiger JR, Valdes ER, Rastogi VK, Knox CK (2017) Deposition method, relative humidity, and surface property effects of bacterial spore reaerosolization via pulsed air jet. Aerosol Sci Technol 51(9):1027–1034. https://doi.org/10.1080/02786826.2017.1335389
Khaled S, Sui R, Charpentier PA, Rizkalla AS (2007) Synthesis of TiO2−PMMA nanocomposite: Using methacrylic acid as a coupling agent. Langmuir 23(7):3988–3995
King MD, McFarland AR (2012) Use of an Andersen bioaerosol sampler to simultaneously provide culturable particle and culturable organism size distributions. Aerosol Sci Technol 46(8):852–861
Kugarajah V, Dharmalingam S (2020) Investigation of a cation exchange membrane comprising sulphonated poly ether ether ketone and sulphonated titanium nanotubes in microbial fuel cell and preliminary insights on microbial adhesion. Chem Eng J 398:125558
Lee S-A, Liao C-H (2014) Size-selective assessment of agricultural workers' personal exposure to airborne fungi and fungal fragments. Sci Total Environ 466–467:725–732. https://doi.org/10.1016/j.scitotenv.2013.07.104
Li H, Cui Q, Feng B, Wang J, Lu X, Weng J (2013) Antibacterial activity of TiO2 nanotubes: influence of crystal phase, morphology and Ag deposition. Appl Surf Sci 284:179–183. https://doi.org/10.1016/j.apsusc.2013.07.076
Liang M, Wang F, Liu M, Yu J, Si Y, Ding B (2019) N-halamine functionalized electrospun poly (vinyl alcohol-co-ethylene) nanofibrous membranes with rechargeable antibacterial activity for bioprotective applications. Adv Fiber Mater 1(2):126–136
Lin C-Y, Li C-S (2002) Control effectiveness of ultraviolet germicidal irradiation on bioaerosols. Aerosol Sci Technol 36(4):474–478
Mainelis G, Willeke K, Adhikari A, Reponen T, Grinshpun SA (2002) Design and collection efficiency of a new electrostatic precipitator for bioaerosol collection. Aerosol Sci Technol 36(11):1073–1085
Manfroi DC, dos Anjos A, Cavalheiro AA, Perazolli LA, Varela JA, Zaghete MA (2014) Titanate nanotubes produced from microwave-assisted hydrothermal synthesis: photocatalytic and structural properties. Ceram Int 40(9):14483–14491
Metcalf AR, Narayan S, Dutcher CS (2018) A review of microfluidic concepts and applications for atmospheric aerosol science. Aerosol Sci Technol 52(3):310–329
Mohraz MH, Golbabaei F, Yu IJ, Mansournia MA, Zadeh AS, Dehghan SF (2019) Preparation and optimization of multifunctional electrospun polyurethane/chitosan nanofibers for air pollution control applications. Int J Environ Sci Technol 16(2):681–694. https://doi.org/10.1007/s13762-018-1649-3
Molina-Reyes J, Romero-Moran A, Uribe-Vargas H, Lopez-Ruiz B, Sanchez-Salas JL, Ortega E, Ponce A, Morales-Sanchez A, Lopez-Huerta F, Zuñiga-Islas C (2020) Study on the photocatalytic activity of titanium dioxide nanostructures: nanoparticles, nanotubes and ultra-thin films. Catal Today 341:2–12
Mollahosseini A, Rahimpour A, Jahamshahi M, Peyravi M, Khavarpour M (2012) The effect of silver nanoparticle size on performance and antibacteriality of polysulfone ultrafiltration membrane. Desalination 306:41–50
Moongraksathum B, Chien M-Y, Chen Y-W (2019) Antiviral and Antibacterial effects of silver-doped TiO2 prepared by the peroxo sol-gel method. J Nanosci Nanotechnol 19(11):7356–7362
Nada A, Moustafa Y, Hamdy A (2014) Improvement of titanium dioxide nanotubes through study washing effect on hydrothermal. Br J Environ Sci 2:29–40
Padiyan DP, Raja DH (2012) Synthesis of various generations titania nanotube arrays by electrochemical anodization for H2 production. Energy Procedia 22:88–100
Plodinec M, Gajović A, Iveković D, Tomašić N, Zimmermann B, Macan J, Haramina T, Su D, Willinger M (2014) Study of thermal stability of (3-aminopropyl) trimethoxy silane-grafted titanate nanotubes for application as nanofillers in polymers. Nanotechnology 25(43):435601
Sahu UK, Mahapatra SS, Patel RK (2018) Application of Box–Behnken design in response surface methodology for adsorptive removal of arsenic from aqueous solution using CeO2/Fe2O3/graphene nanocomposite. Mater Chem Phys 207:233–242
Saleh TA, Gupta VK (2012) Photo-catalyzed degradation of hazardous dye methyl orange by use of a composite catalyst consisting of multi-walled carbon nanotubes and titanium dioxide. J Colloid Interface Sci 371(1):101–106
Santos A, Bedrikovetsky P (2004) Size exclusion during particle suspension transport in porous media: stochastic and averaged equations. Comput Appl Math 23(2–3):259–284
Selvam AK, Nallathambi G (2015) Polyacrylonitrile/silver nanoparticle electrospun nanocomposite matrix for bacterial filtration. Fibers Polym 16(6):1327–1335. https://doi.org/10.1007/s12221-015-1327-8
Seo D-S, Lee J-K, Kim H (2001) Preparation of nanotube-shaped TiO2 powder. J Cryst Growth 229(1–4):428–432
Shah LA, Malik T, Siddiq M, Haleem A, Sayed M, Naeem A (2019) TiO2 nanotubes doped poly (vinylidene fluoride) polymer membranes (PVDF/TNT) for efficient photocatalytic degradation of brilliant green dye. J Environ Chem Eng 7(5):103291
Su EP, Justin DF, Pratt CR, Sarin VK, Nguyen VS, Oh S, Jin S (2018) Effects of titanium nanotubes on the osseointegration, cell differentiation, mineralisation and antibacterial properties of orthopaedic implant surfaces. Bone Joint J 100(1_Supple_A):9–16
Tabe S (2014) Electrospun nanofiber membranes and their applications in water and wastewater treatment. In: Nanotechnology for Water Treatment and Purification. Springer, Cham, pp 111–143
Tiyek I, Gunduz A, Yalcinkaya F, Chaloupek J (2019) Influence of electrospinning parameters on the hydrophilicity of electrospun polycaprolactone nanofibres. J Nanosci Nanotechnol 19(11):7251–7260
Van Viet P, Thi CM (2016) The directed preparation of TiO 2 nanotubes film on FTO substrate via hydrothermal method for gas sensing application. AIMS Mater Sci 3(2):460–469
Wang N, Wang X, Ding B, Yu J, Sun G (2012) Tunable fabrication of three-dimensional polyamide-66 nano-fiber/nets for high efficiency fine particulate filtration. J Mater Chem 22(4):1445–1452. https://doi.org/10.1039/c1jm14299b

Wang G, Feng H, Hu L, Jin W, Hao Q, Gao A, Peng X, Li W, Wong K-Y, Wang H, Li Z, Chu PK (2018) An antibacterial platform based on capacitive carbon-doped TiO2 nanotubes after direct or alternating current charging. Nat Commun 9(1):2055. https://doi.org/10.1038/s41467-018-04317-2

Xu J-C, Lu M, Guo X-Y, Li H-L (2005) Zinc ions surface-doped titanium dioxide nanotubes and its photocatalysis activity for degradation of methyl orange in water. J Mol Catal A Chem 226(1):123–127

Yu K-P, Lee GW-M, Lin S-Y, Huang CP (2008) Removal of bioaerosols by the combination of a photocatalytic filter and negative air ions. J Aerosol Sci 39(5):377–392

Yuan Z-Y, Su B-L (2004) Titanium oxide nanotubes, nanofibers and nanowires. Colloids Surf A Physicochem Eng Asp 241(1–3):173–183

Zhang L, Li L, Wang L, Nie J, Ma G (2020) Multilayer electrospun nanofibrous membranes with antibacterial property for air filtration. Appl Surf Sci 515:145962

Zhao C, Feng B, Li Y, Tan J, Lu X, Weng J (2013) Preparation and antibacterial activity of titanium nanotubes loaded with Ag nanoparticles in the dark and under the UV light. Appl Surf Sci 280:8–14

Zhu M, Hua D, Pan H, Wang F, Manshian B, Soenen SJ, Xiong R, Huang C (2018) Green electrospun and crosslinked poly (vinyl alcohol)/poly (acrylic acid) composite membranes for antibacterial effective air filtration. J Colloid Interface Sci 511:411–423

Zucolotto V, Avlyanov J, Gregorio R Jr, Mattoso LHC (2004) Melt processing of composites of PVDF and carbon black modified with conducting polymers. J Appl Polym Sci 94(2):553–557